RSC Advances

PAPER

View Article Online
View Journal | View Issue

Cite this: *RSC Adv.*, 2024, **14**, 27204

Novel Fe/Ca oxide co-embedded coconut shell biochar for phosphorus recovery from agricultural return flows†

Anqi Hu,‡[ac] Yongcan Jiang,‡*[ab] Jiaqi An,[c] Xiaodian Huang,[a] Abdelbaky Hossam Elgarhy,[cd] Huafen Cao[c] and Guanglong Liu *[c]

Efficient elimination and recovery of phosphorus from agricultural return flows are crucial for effective eutrophication management and phosphorus reuse. In this study, a neutral Fe/Ca oxide co-embedded biochar (FCBC) was synthesized using calcium peroxide and ferrous chloride as precursors for phosphate recovery from agricultural return flows. FCBC possesses a highly intricate pore structure and an abundance of surface-active groups. Fe/Ca oxides were loaded onto the biochar in the form of $Ca_2Fe_2O_5$, Fe_2O_3, and $CaCO_3$. FCBC demonstrated a broad pH tolerance range (pH = 6–12) in the aquatic environment. The maximum saturation adsorption capacity was 53.31 mg g^{-1}. Phosphorus removal is influenced by $Ca_3(PO_4)_2$ generation, intra-particle diffusion, and electrostatic attraction. The produced FCBC showed exceptional phosphorus removal efficiency in the presence of various anions, except for wastewater with high concentrations of SO_4^{2-}, CO_3^{2-}, HCO_3^-, and F^- (>500 mg L^{-1}). FCBC can effectively remove phosphorus from agricultural return flows and reduce the risk of the water environment. Returning it to the field can also mitigate the depletion of phosphorus resources, effectively reduce carbon emissions from farmland, improve soil fertility, and realize multiple benefits.

Received 2nd July 2024
Accepted 16th August 2024

DOI: 10.1039/d4ra04795h

rsc.li/rsc-advances

1 Introduction

Phosphorus is a vital macronutrient for the growth of crops.[1,2] However, the loss of large amounts of phosphorus from agricultural return flows can lead to eutrophication of water bodies, loss of aquatic biodiversity, and the destruction of ecosystems.[3–5] Furthermore, phosphorus compounds are non-renewable and irreplaceable materials that are in limited supply.[6] It is crucial to extract and reclaim phosphorus from agricultural return flows before their release into water bodies.[7]

Phosphorus elimination from aquatic environments is commonly done using methods including chemical precipitation,[8] microbial processes,[9] membrane filtration,[10] and adsorption.[11] Adsorption is a highly utilized method for removing phosphorus, known for its versatility in using various adsorbent materials, rapid phosphorus adsorption rates, excellent selectivity, low cost, and renewability.[12–14] Biochar is a highly promising adsorbent that is obtained from converting biomass through thermochemical processes without oxygen.[15–17] It consists of functional groups such as hydroxyl, carboxyl, and aromatic groups.[18] Biochar is extensively utilized for the treatment of pharmaceuticals, heavy metals, and inorganic contaminants in wastewater.[19–21] However, the biochar prepared from different raw materials varies greatly.[22] For example, straw, grain hulls, and peanut shells are not mechanically strong enough, resulting in the prepared biochar being easily pulverized during actual use, thus causing the clogging of agricultural return flows. Coconut is a tropical crop widely grown in Hainan, China, with an annual production of up to one billion pieces, a large number of coconut shells can serve as raw material for biochar production. Moreover, biochar made from coconut shells, which offers excellent structural strength and high cost-effectiveness, is easy to obtain.[23]

In addition, the capability of biochar to eliminate phosphate from liquids is limited by the substantial negative charge on its surface, which reduces its ability to adsorb anions.[24,25] Therefore, researchers usually chemically modify biochar to improve its capacity to adsorb phosphates in aqueous solutions.[26,27] Liu *et al.* utilized Mg/Fe bimetallic oxides to modify waste straw biochar to produce Mg/Fe biochar for extracting phosphate from simulated urine as a phosphate fertilizer.[28] Palansooriya

[a]*PowerChina Huadong Engineering Corporation Ltd., Hangzhou 311122, Zhejiang Province, China*

[b]*Institute of Soil and Water Resources and Environmental Science, College of Environmental and Resource Sciences, Zhejiang University, Hangzhou 310058, Zhejiang Province, China*

[c]*State Environmental Protection Key Laboratory of Soil Health and Green Remediation, College of Resources and Environment, Huazhong Agricultural University, Wuhan 430070, China. E-mail: liugl@mail.hzau.edu.cn*

[d]*Central Laboratory for Environmental Quality Monitoring (CLEQM), National Water Research Center (NWRC), Qalyobia, 13621, Egypt*

† Electronic supplementary information (ESI) available. See DOI: https://doi.org/10.1039/d4ra04795h

‡ Contributed equally to this work.

et al. produced Fe(III) loaded chitosan–biochar composite fibers using paper mill sludge biochar produced at 600 °C in N_2 and CO_2 environments.[29] Wang *et al.* produced several biochars by pyrolyzing oak sawdust with or without the addition of $LaCl_3$ and discovered that the phosphorus adsorption efficiency of oak sawdust biochars (pyrolyzed at 500 °C) increased from 10.44 mg g^{-1} for unmodified biochars to 46.57 mg g^{-1} for La-modified biochars.[30] Modifying biochar with metal oxides is anticipated to enhance its surface structure and produce functional biochar materials. Fe is widely distributed in nature, and its structural properties are favorable for phosphate to undergo ion exchange and ligand complexation on the surface of this type of adsorbent. Research has shown that incorporating iron into biochar can boost the positive surface charge,[31] leading to improved anion exchange capacity and enhanced redox performance.[32,33] In our previous watershed agri-environmental management project, iron-loaded biochar was industrially produced by impregnation with ferrous chloride ($FeCl_2$) and used to remove phosphorus from agricultural return flows. However, the adsorbents produced were typically acidic, which limited their practical application. To address this issue, CaO_2 was introduced in this study, which contains high-energy peroxide covalent bonds and generates basic calcium hydroxide plus oxygen when in contact with water.[34] CaO_2 is a metal-based peroxide commonly explored as an environment-friendly oxygen-releasing compound that exhibits greater stability, sustainability, efficiency, and cost-effectiveness.[35–37] Meanwhile, CaO_2 can oxidize divalent iron to trivalent iron and generate Fe/Ca oxides on biochar.

The study aimed to (1) produce a novel Fe/Ca oxide co-embedded modified biochar (FCBC) from coconut shell biochar with $FeCl_2$ and CaO_2 as precursors; (2) analyze the structural properties of biochar through material characterization; (3) investigate the adsorption effect and removal mechanism of FCBC on phosphorus in solution; and (4) determine the potential of FCBC for phosphorus recovery from agricultural return flows. This study provides a technical reserve for the prevention and control of agricultural surface pollution.

2 Materials and methods

2.1. Preparation of modified biochars

Coconut shell biochar is mass-produced by China Zhengzhou Bamboo Forest Activated Carbon Development Company. The production process involves cleaning the collected coconut shells, removing dust and impurities, cutting and crushing them into appropriate sizes, drying them, and then pyrolyzing and carbonizing the dried coconut shell residue to produce coconut-shell biochar (BC).

BC of 4–10 mesh size was impregnated in a $FeCl_2$ (0.5 M) solution and the pH was adjusted to about 7 utilizing CaO_2 powder. The solution containing the mixture of iron and calcium was oscillated at 20 °C and 200 rpm for 12 hours. The iron and calcium mixture was evenly distributed on the coconut shell biochar by oscillation. The biochar was removed after oscillation and dried at 70 °C until the modified material reached a stable state, which was then placed in a muffle furnace and pyrolyzed at 300, 400, 500, 600, 700, 800, and 900 °C for 1 h, separately, to obtain Fe/Ca oxide co-embedded modified biochar (FCBC) prepared at different pyrolysis temperatures. The reaction chemical equations are depicted in eqn (1)–(3):[38]

$$2CaO_2 + 2H_2O \rightarrow 2Ca(OH)_2 + O_2\uparrow \quad (1)$$

$$FeCl_2 + Ca(OH)_2 \rightarrow Fe(OH)_2\downarrow + CaCl_2 \quad (2)$$

$$4Fe(OH)_2 + O_2 + 2H_2O \rightarrow 4Fe(OH)_3\downarrow \quad (3)$$

2.2. Material characterization

The surface morphology and elemental composition of materials were characterized utilizing a scanning electron microscope-energy dispersive spectrometer (SEM-EDS, Hitachi S4800). The specific surface area, pore volume, and pore size of materials were determined utilizing a surface area analyzer (BET, Micromeritics ASAP 2460). The crystal structures of BC and FCBC before and after phosphorus adsorption were analyzed utilizing X-ray diffraction (XRD, Bruker D8) at a scan rate of 10° min^{-1} and an acquisition range of 10–90°. Fourier transform infrared absorption spectroscopy (FT-IR, Bruker Nicolet IS10) was utilized to determine the characteristic functional groups on the surfaces of BC and FCBC before and after phosphorus adsorption. The surface elemental compositions and electronic states of BC and FCBC before and after the adsorption of phosphorus were examined utilizing X-ray photoelectron spectroscopy (XPS, Thermo escalab 250XI). The charge zero point (pH_{ZPC}) of FCBC was analyzed using the pH-drift method.[39]

2.3. Adsorption experiments

250 mL of phosphorus solution with a certain amount of biochar was added to a 500 mL conical flask, placed on a thermostatic oscillator, and the adsorption was oscillated for 12 h at a temperature of 20 °C and a speed of 150 rpm. After adsorption, the solution was filtered through a 0.45 μm membrane, and then the concentration of phosphorus in the remaining solution was determined by ammonium molybdate spectrophotometry at 700 nm. All experiments were repeated three times.

The effects of adsorbent dosage (0.1–8 g L^{-1}), pH (2–12), adsorption time (0–24 h), initial phosphorus concentration (5–500 mg L^{-1}), and coexisting ions (Cl^-, NO_3^-, F^-, SO_4^{2-}, HCO_3^-, and CO_3^{2-}) on phosphorus adsorption were investigated. Finally, the phosphorus removal from agricultural return flows by modified biochar was determined. The specific experimental steps are shown in Text S1.†

3 Results and discussion

3.1. Characterization of biochar

The N_2 adsorption–desorption curve (Fig. S1a†) of BC and FCBC exhibited a distinct type IV isotherm with a hysteresis loop ($0.40 < P/P_0 < 1.0$), indicating that the mesoporous structure existed in

BC and FCBC.[40] The narrow pore size distribution pattern (Fig. S1b†) based on Barret–Joyner–Halenda (BJH) further illustrates the mesoporous structure of the two biochars. As indicated in Table S1,† the specific surface area of biochar rise from 291.29 $m^2 g^{-1}$ to 441.52 $m^2 g^{-1}$, and the micropore volume from 0.2186 $cm^3 g^{-1}$ to 0.2640 $cm^3 g^{-1}$ after modification, thus promoting the adsorption of phosphorus by FCBC.

The microstructures of BC and FCBC were analyzed using SEM (Fig. 1). At the microscopic scale, after magnifications of 2 K and 10 K, the surface of the BC (Fig. 1a and b) appeared relatively flat and loaded with flaky debris of varying sizes. After the modification of the biochar (Fig. 1c and d), surface-loaded particles were observed, forming an intricate pore structure. In summary, the introduction of Ca/Fe modified the surface morphology of the biochar, increasing the pore structure and specific surface area. The C, O, Ca, and Fe contents on the surface of BC (Fig. 1e) and FCBC (Fig. 1f) were analyzed by EDS, and the spectra of the surface elements on both biochars are

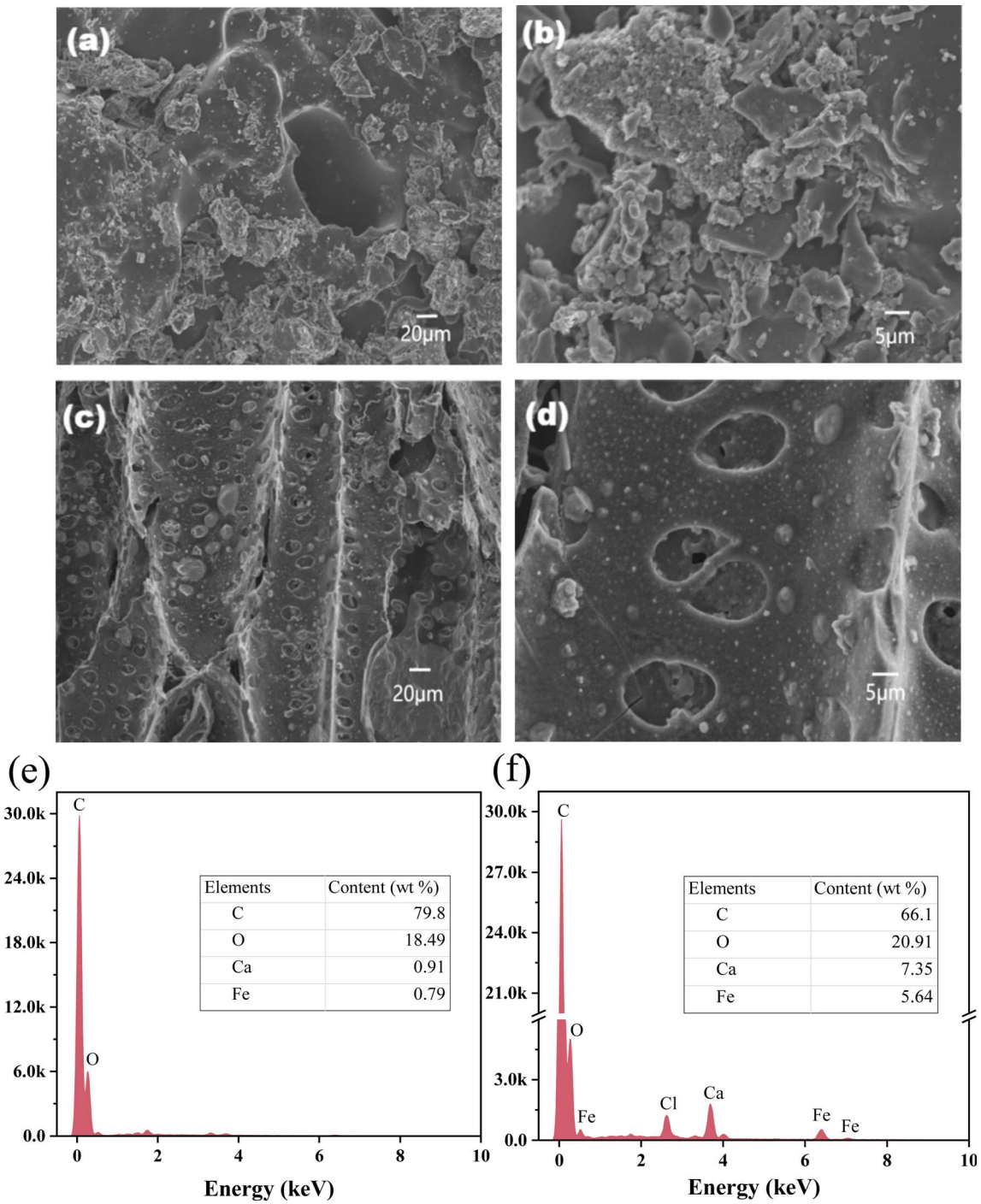

Fig. 1 SEM images of BC (a and b), and FCBC (c and d) at different magnifications; EDS analysis of BC (e) and FCBC (f).

shown in Fig. S2.† After modification, a decrease in the mass percentage of C from 79.80% to 66.10%, and the introduction of additional forms of O, including Ca–O, Fe–O, and C–O, resulted in an increase in the mass percentage of O from 18.49% to 20.91%. Simultaneously, the mass percentage of Ca increased from 0.91% to 7.35%, while the mass percentage of Fe ascended from 0.79% to 5.64%. The elevated levels of Fe, Ca, and O demonstrate the effective deposition of Fe/Ca oxides onto the modified biochar.

XRD analysis was used to examine BC and FCBC before and after phosphorus adsorption (Fig. 2a). Characteristic peaks appeared at 2θ angles of 24.3° and 43.1° for both BC and FCBC. However, the intensities of the characteristic bands after modification were considerably reduced compared with those of the biochar before modification. The broad packing peak at 24° for BC and FCBC was associated with amorphous C. Additionally, $CaCO_3$ (JCPDS no. 05-0586) and Fe_2O_3 (JCPDS no. 24-0072) were detected, suggesting that the interaction between CaO_2 and C produced $CaCO_3$, while $FeCl_2$ was predominantly converted to hematite Fe_2O_3 during the modification process.[41,42] Furthermore, $Ca_2Fe_2O_5$ (JCPDS no. 47-1744) was present as a result of the combination of $FeCl_2$ and CaO_2 demonstrating the successful production of Fe/Ca oxide co-embedded biochar.[43] After the adsorption of phosphorus on FCBC (P-FCBC), Ca was present as $Ca_3(PO_4)_2$ (JCPDS no. 17-0500) on the modified biochar, indicating that phosphate was complexed with Ca^{2+} on the FCBC.

Fig. 2b displays the FT-IR spectra of BC and FCBC before and after phosphorus adsorption. The broad band at 3448 cm^{-1} represents the telescopic vibrational absorption band of O–H. In BC, the absorption band at 1627 cm^{-1} indicates the C–H stretching vibration of aromatic hydrocarbons, while the absorption band at 1565 cm^{-1} corresponds to the stretching vibration of the C=C double bond. After modification, the FCBC group underwent a shift, resulting in the appearance of C–H at 1646 cm^{-1} and a C=C double bond absorption band at 1509 cm^{-1}. Additionally, new infrared absorption bands emerged, including the characteristic absorption band of Ca–O at 877 cm^{-1} and the telescopic vibrational absorption bands of Fe–O at 466 cm^{-1} and 603 cm^{-1}. These results further demonstrate the successful loading of Fe/Ca oxides onto FCBC. After phosphorus adsorption, the bands at 1049 cm^{-1} and 565 cm^{-1} in P-FCBC intensified due to the stretching of the P–O bond. These bands indicate that phosphate has been effectively adsorbed onto FCBC.[44,45]

Fig. S3† illustrates the C 1s (a) and O 1s (b) XPS spectra of BC. The XPS total spectra of FCBC and P-FCBC (Fig. 2c) revealed that the predominant components on the surface of FCBC were Ca, Fe, O, and C, with a lower amount of Fe considered to be encapsulated. The successful adsorption of phosphate was verified by the observation of a P 2p peak with a binding energy of 133.9 eV after phosphorus adsorption, and the phosphorus content of P-FCBC was increased to 6.12%. FCBC contained a significant amount of Ca before phosphorus adsorption (Fig. 2f), as indicated by the peaks at 347.9 eV and 351.5 eV, which represented the Ca 2p1/2 and 2p3/2 orbitals of $CaCO_3$. The existence of metal-phosphate peaks at 349.0 eV and 352.5 eV after phosphorus adsorption indicated the production of $Ca_3(PO_4)_2$ on the surface of FCBC, which aligns with the XRD findings. As depicted in Fig. 2e, before phosphorus absorption, the O 1s peak in FCBC exhibits three distinct peaks: C=O/CO_3^{2-} (531.5 eV), C–O–C/C–O–H (532.0 eV), and C=O–O* (533.5 eV). The proportion of C–O–C/C–O–H bonds rose from 44.14% to 66.33% following adsorption. The rehydration of the FCBC mostly caused this reaction. Several M–O bonds within the metal oxides undergo conversion to M–OH, increasing the number of hydroxyl functional groups.[46] The C 1s spectrum (Fig. 2d) demonstrated a reduction in the proportion of CO_3^{2-} from 8.89% to 3.32% after the adsorption of phosphorus by FCBC, indicating that $CaCO_3$ was mainly converted to $Ca_3(PO_4)_2$ attached to the surface of the biochar.

3.2. Adsorption of phosphorus by biochar

3.2.1. Effect of dosage and initial pH on phosphorus adsorption. As illustrated in Fig. S4,† the phosphorus adsorption capacity of FCBC consistently rose with rising pyrolysis temperature and reached a maximum at 800 °C (21.98 mg g^{-1}). When the temperature is higher than 800 °C, the adsorption capacity is slightly weakened. Cui *et al.* revealed that the specific surface area of biochar made from different wetland plants grew from 2.08–10.65 m^2 g^{-1} to 50.05–281.15 m^2 g^{-1} as the pyrolysis temperature rose from 300 °C to 600/700 °C.[47] When the pyrolysis temperature exceeds a certain level, the organic macromolecules (such as proteins, carbohydrates, and lipids) of biochar are destroyed.[48] Therefore, 800 °C was selected as the ideal pyrolysis temperature for following investigation. According to Fig. 3a, the adsorption capacity of BC was lower than 0.03 mg g^{-1} at various dosages. The phosphorus adsorption capacity of FCBC rose as the dosage escalated from 0.1 g L^{-1} (14.86 mg g^{-1}) to 2 g L^{-1} (19.89 mg g^{-1}) but decreased for dosages over 2 g L^{-1}. The increased amount of FCBC initially raised the adsorption capacity by providing more adsorption sites on the FCBC surface for phosphate interaction. As the dosage increased, the amount of adsorption sites surpassed the required level for phosphate interaction. This observation aligns with the study conducted by Zou *et al.*[49] The underutilization of adsorption sites causes a reduced adsorption capacity per unit mass of biochar.[50] Therefore, 2 g L^{-1} was considered to be the ideal dose for subsequent study.

The initial pH of the solution plays a crucial role in controlling phosphate removal. Fig. 3b demonstrates that the phosphorus adsorption capability of FCBC increased as the pH value rose. The adsorption capacity of FCBC at pH = 2 (5.44 mg g^{-1}) and 4 (10.83 mg g^{-1}) was significantly lower than that for phosphorus at pH 6 to 12 ($p < 0.05$). There was no significant disparity in the adsorption capacity of phosphorus at initial pH values of 8 and 10 ($p > 0.05$). The highest adsorption capacity of 21.28 mg g^{-1} was obtained at an initial pH value of 12. The results showed that FCBC exhibited significant adsorption even in alkaline environments, indicating a good pH adaptation range. The phosphate adsorption capacity is influenced by the form of phosphate and the surface charge of the biochar.[50] As shown in Fig. S5,† the predominate forms of phosphate at

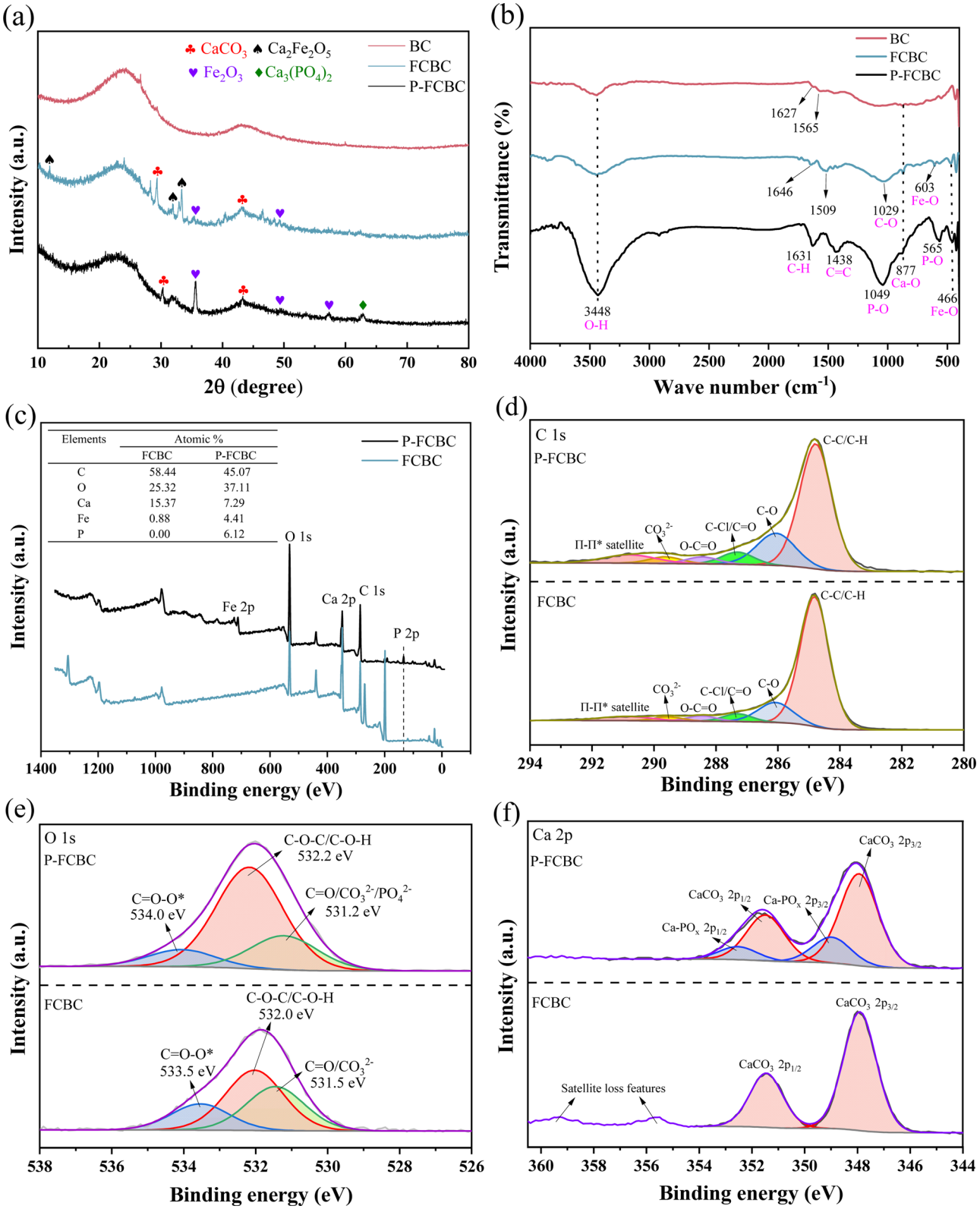

Fig. 2 XRD patterns (a) and FT-IR spectra (b) of BC, FCBC, and P-FCBC. XPS analysis of FCBC and P-FCBC: XPS total spectra (c), C 1s (d), O 1s (e), Ca 2p (f).

various pH are H_3PO_4 (pH < 2.16), $H_2PO_4^-$ (pH = 2.16–7.21), HPO_4^{2-} (pH = 7.21–12.31), and PO_4^{3-} (pH > 12.32). The solution started with a pH of 2 and ended with a pH of 2.04. The primary phosphate species present at pH 2–2.04 was $H_2PO_4^-$, which was unable to combine with Ca^{2+} and Fe^{2+} to generate a precipitate, leading to the lowest adsorption capacity. With an

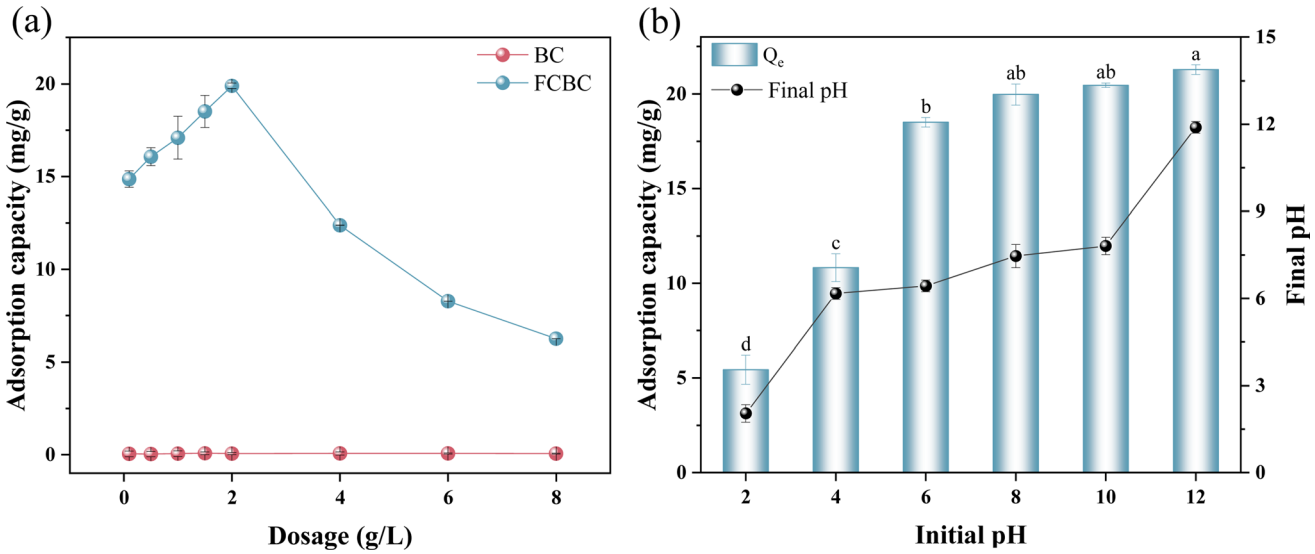

Fig. 3 Adsorption effects of BC and FCBC on phosphorus at different dosages (a); the influence of solution's initial pH on adsorption capacity for phosphorus and final pH (b), distinct letters represent significant variations in adsorption at various pH levels ($p < 0.05$, Duncan's test).

initial pH of 6–12, the final pH of the solution ranged from 6.43 to 11.89, with HPO_4^{2-} being the predominant form, and the form of HPO_4^{2-} tended to react with Ca^{2+} and precipitate on FCBC.[51,52] There was very little change in pH before and after adsorption, indicating that FCBC had no significant effect on solution pH. Fig. S6† illustrates the zero point charge (pH_{ZPC}) of FCBC as 7.41, with a prevalence of positive charges below pH_{ZPC}. Therefore, electrostatic attraction might be the primary mechanism by which FCBC adsorbs phosphate at pH < 7.41.[53]

3.2.2. Adsorption kinetics and isotherms. The kinetics of phosphate adsorption by FCBC was simulated using pseudo-first-order, pseudo-second-order (Fig. 4a), and intra-particle diffusion models (Fig. 4b). The pseudo-second-order model ($R^2 = 0.9939$) outperforms the pseudo-first-order model ($R^2 = 0.9844$) (Table S2†), indicating that phosphorus adsorption of FCBC is a chemisorption procedure involving covalent forces between electron sharing and exchange. FCBC achieved adsorption equilibrium in 600 min with an adsorption capacity of 22.28 mg g^{-1}. Fig. 4b demonstrates three well-fitted stages in the adsorption process ($R^2 > 0.99$). During the initial stage, phosphate is transferred from the solution to the outer surface of FCBC due to the concentration gradient of phosphate and electrostatic adsorption. The following stage entails the intra-particle diffusion process when phosphate moves from the outer surface to the inner surface of the FCBC through pore diffusion. The final stage is the adsorption equilibrium stage. The linear curve did not intersect the origin, suggesting that factors other than intra-particle diffusion were restricting the adsorption rate.[54]

The adsorption isotherm of FCBC was investigated by varying the initial phosphate concentration. The phosphate adsorption capability of FCBC was assessed by applying the Langmuir and Freundlich models (Fig. 4c). Table S3† indicates that the Langmuir model outperforms the Freundlich model, with R^2 values of 0.9982 and 0.9631, respectively. The maximal adsorption capacity obtained from the Langmuir fit is 53.31 mg g^{-1}. The phosphorus adsorption mechanism of FCBC involves monomolecular layer chemisorption,[55] indicating that the adsorption sites of the modified biochar are stationary and evenly dispersed, with no interaction occurring between the adsorbed phosphate ions. Table S4† displays a comparison of the highest phosphorus adsorption capacity by different biochar adsorbents, FCBC was higher than the other similar adsorbents. Furthermore, the $1/n$ value derived from the Freundlich model was within the range of 0.1 to 0.5, suggesting that the adsorption of phosphate by FCBC was readily achievable.[56]

3.2.3. Effect of coexisting anions on phosphorus adsorption. Common anions in natural water and wastewater can vie with phosphorus for adsorption sites on biochar.[57] Fig. 4d reveals the influence of various anions on the phosphorus adsorption capacity of FCBC. The adsorption capacity of FCBC was considerably greater in the presence of NO_3^- and Cl^- in comparison with the other treatment groups ($p < 0.05$). These results indicate that the existence of NO_3^- and Cl^- had no significant detrimental impact on phosphorus removal by the FCBC. The presence of SO_4^{2-}, CO_3^{2-}, HCO_3^-, and F^- significantly inhibited the phosphorus absorption capacity of FCBC, and the inhibitory effects of these anions became more pronounced as the concentration rose from 100 to 1000 mg L^{-1}. This is might due to the competitive formation of $FeCO_3$ ($K_{sp} = 3.5 \times 10^{-11}$), $CaCO_3$ ($K_{sp} = 3.8 \times 10^{-9}$), and $CaSO_4$ ($K_{sp} = 9.1 \times 10^{-6}$), *etc.*, where the presence of CO_3^{2-} and SO_4^{2-} ions can occupy some of the adsorption sites. Furthermore, F^- is highly electronegative.[58] Zhang *et al.* studied the effect of fluoride on the surface of γ-alumina using multinuclear MAS-NMR spectroscopy to determine the fluorine compounds present on the fluorinated γ-alumina.[59] When exposed to higher fluoride levels, the bridging Al–O–Al bonds are disrupted to absorb more fluoride due to the powerful electron-withdrawing influence of

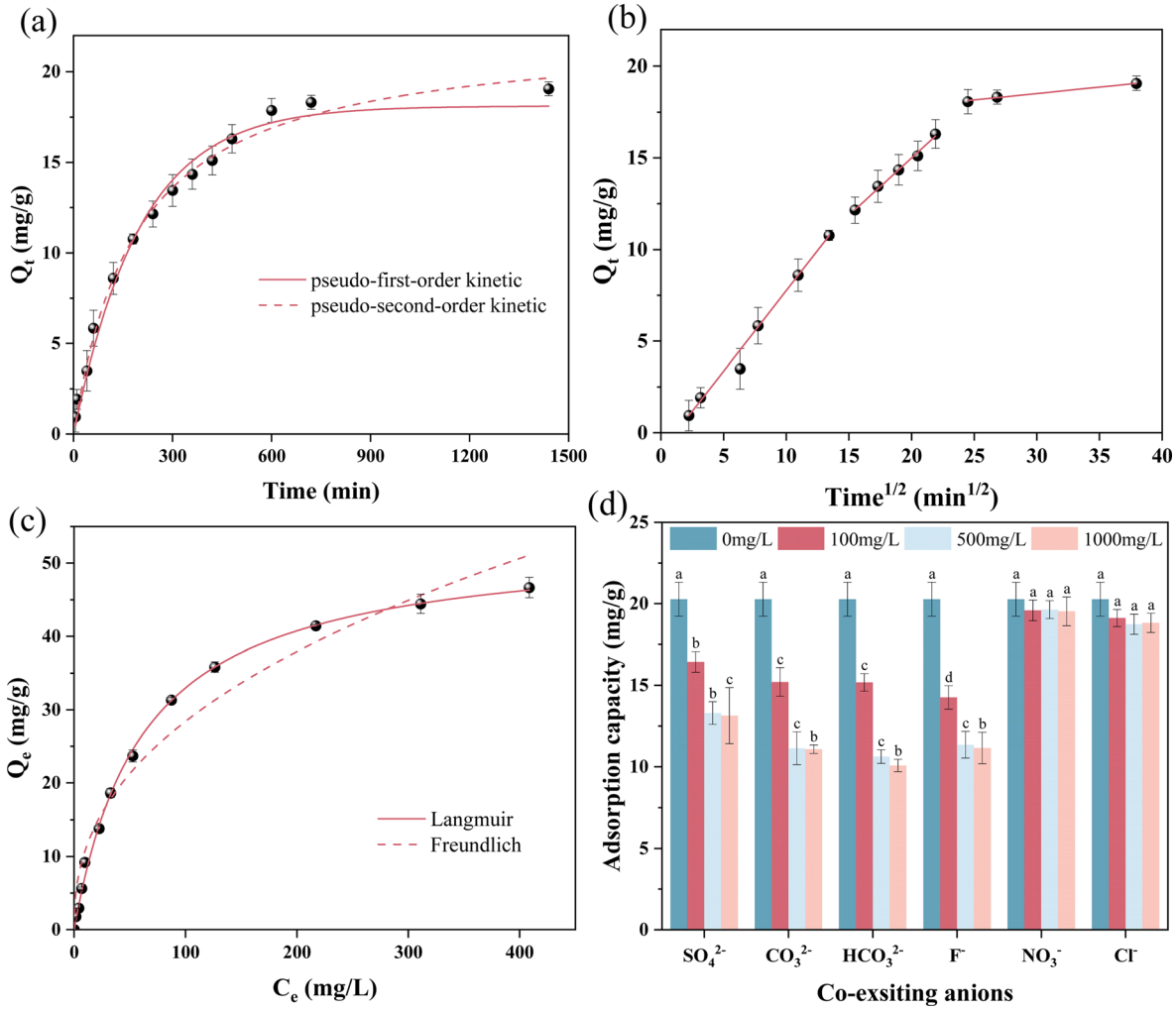

Fig. 4 Kinetics of phosphate adsorption on FCBC: pseudo-first-order, pseudo-second-order (a), and intra-particle diffusion model (b). Adsorption isotherm for phosphorus on FCBC(c). Effect of co-existing anions on the phosphorus adsorption of FCBC (d), different letters assigned to the same concentration indicate significant variations in the removal rates of different coexisting ions ($P < 0.05$, Duncan's test).

fluorine. The presence of F^- substantially reduced the adsorption of phosphate. Similar processes are anticipated to occur in FCBC. Accordingly, the prepared FCBC exhibited excellent phosphorus removal capacity under complex conditions of multiple anion coexistence, except for water containing high concentrations of SO_4^{2-}, CO_3^{2-}, HCO_3^-, and F^- (*i.e.*, >500 mg L^{-1}).

3.2.4. Mechanism of phosphorus adsorption by FCBC. The adsorption mechanism of phosphorus by FCBC is illustrated in Fig. 5, encompassing primarily the following: (1) electrostatic attraction. When the pH is below the isoelectric point (pH_{ZPC} = 7.41), the hydroxyl groups on the surface of FCBC become protonated and provide an electrostatic attraction to phosphate anions in solution. (2) Intra-particle diffusion. Phosphate anions are initially trapped by the adsorption sites on the surface of the adsorbent and subsequently penetrate the internal channels of the FCBC by intra-particle diffusion. Based on the intra-particle diffusion model, the adsorption process can be categorized into three distinct phases. Among these phases, the intra-particle diffusion phase is the primary factor that restricts the adsorption rate. (3) Ligand exchange. The XPS examination detected the conversion of M–O to M–OH on the FCBC surface. During the process of ligand exchange, the hydroxyl groups were substituted with phosphate groups in solution, resulting in the formation of inner-sphere complexation through the bonding of metal atoms to phosphate molecules.[60]

3.3. Removal of phosphorus by modified biochar from agricultural return flows

To investigate the impact of FCBC on the adsorption of phosphorus from agricultural return flows, three sampling sites were selected for this study: pond, farmland, and ditch. The water samples' physical and chemical parameters are detailed in Table S5.† According to Fig. 6, the initial total phosphorus concentrations of the water samples collected from the pond, farmland, and ditch were 0.34 mg L^{-1}, 0.53 mg L^{-1}, and 0.11 mg L^{-1}, respectively. There was no significant variation in

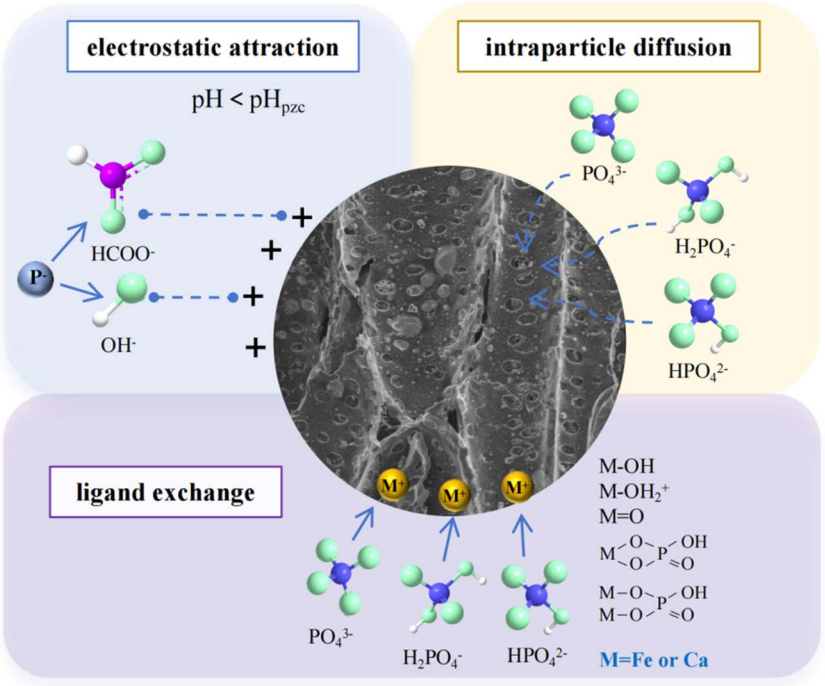

Fig. 5 Mechanism of phosphorus adsorption by FCBC.

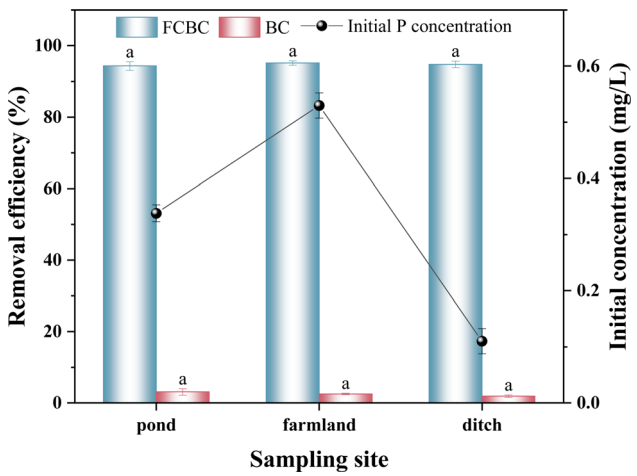

Fig. 6 Phosphorus removal effect of BC and FCBC on pond, farmland, and ditch water, different letters for the same type of biochar indicate significant differences in removal efficiency at different sampling sites (P < 0.05, Duncan's test).

the phosphorus removal effectiveness of BC among the three water samples (p > 0.05), all of which were below 3%. In contrast, the phosphorus removal efficiency of FCBC did not differ significantly (p > 0.05) among the three water samples, with values of 94.32%, 95.12%, and 94.74% respectively. The results demonstrate that FCBC is highly effective at eliminating phosphorus from agricultural return flows. The phosphorus content on the surface of P-FCBC saturated with phosphorus is about 6.12% (Fig. 3a). Phosphorus is a crucial ingredient for plant development. Hence, waste FCBC has good prospects for agricultural applications as a soil conditioner and fertilizer. Fang *et al.* prepared a novel magnesium oxide-rich composite biochar (MFBC) directly by co-pyrolyzing magnesite with food waste and applied P-MFBC saturated with phosphorus to the soil, the results showed that P-MFBC can slowly release phosphorus in the soil and has the value of fertilizer use.[61] Li *et al.* discovered that incorporating phosphorus-loaded nano-CaO_2/BC composites into soil might enhance soil quality and stimulate the growth of tomato seedlings.[62] In summary, utilizing FCBC to eliminate phosphorus from agricultural wastewater can reduce agricultural surface pollution, and the recovered FCBC can be utilized in the field to improve soil fertility. In addition, the effects of FCBC on plant growth and soil metal accumulation require further research to clarify the ecological risks posed by FCBC.

4 Conclusions

Novel Fe/Ca oxide co-embedded modified biochar (FCBC) was successfully produced using coconut-shell biochar as the raw material. FCBC exhibited a phosphorus adsorption capacity ranging from 18.50 to 21.28 mg g^{-1} within an initial pH range of 6 to 12. Based on Langmuir model, the maximum adsorption capacity of FCBC was 53.31 mg g^{-1} at dosage of 2 g L^{-1}, pH 7, and temperature of 20 °C. The mechanisms of phosphorus adsorption by FCBC entail electrostatic attraction, intra-particle diffusion, and ligand exchange. The phosphorus removal effects of FCBC in agricultural return flows exceeded 94%. Therefore, FCBC exhibits significant promise as an eco-friendly and cost-effective modified biochar to eliminate phosphate from water bodies and has the potential to be utilized as a soil supplement and slow-release fertilizer.

Data availability

The data supporting this article have been included as part of the ESI.†

Author contributions

Anqi Hu: writing – original draft, writing – review & editing, data curation, visualization, formal analysis, conceptualization, methodology, investigation. Yongcan Jiang: writing – review & editing, supervision, funding acquisition. Jiaqi An: writing – review & editing, validation. Xiaodian Huang: funding acquisition. Abdelbaky Hossam Elgarhy: writing – review & editing. Huafen Cao: supervision. Guanglong Liu: resources, supervision, writing – review & editing.

Conflicts of interest

The authors have no relevant financial or non-financial interests to disclose.

Acknowledgements

This research was supported by the Science and Technology Project of the Huadong Engineering (Fujian) Corporation (ZKY2022-FJ-02-02).

References

1 B. K. Mayer, L. A. Baker, T. H. Boyer, P. Drechsel, M. Gifford, M. A. Hanjra, P. Parameswaran, J. Stoltzfus, P. Westerhoff and B. E. Rittmann, Total Value of Phosphorus Recovery, *Environ. Sci. Technol.*, 2016, **50**, 6606–6620, DOI: **10.1021/acs.est.6b01239**.

2 H. Zhang, Y. Yang, F. Chen, D. Liu, R. Zhu and S. Wu, Removal and recovery of phosphorus by a long–term stabilized amorphous calcium carbonate, *Sep. Purif. Technol.*, 2024, **350**, 127956, DOI: **10.1016/j.seppur.2024.127956**.

3 F. Yang, S. Zhang, Y. Sun, D. C. W. Tsang, K. Cheng and Y. S. Ok, Assembling biochar with various layered double hydroxides for enhancement of phosphorus recovery, *J. Hazard. Mater.*, 2019, **365**, 665–673, DOI: **10.1016/j.jhazmat.2018.11.047**.

4 H. Chen, J. H. Yuan, G. L. Chen, X. Zhao, S. Q. Wang, D. J. Wang, L. Wang, Y. J. Wang and Y. Wang, Long-term biochar addition significantly decreases rice rhizosphere available phosphorus and its release risk to the environment, *Biochar*, 2022, **4**, 15, DOI: **10.1007/s42773-022-00178-7**.

5 X. Song, X. Chen, W. Q. Chen and T. Q. Ao, ZrO2 nanoparticles embedded in biochar modified with layered double oxides nanosheets for phosphorus removal by capacitive deionization, *Sep. Purif. Technol.*, 2024, **328**, 10, DOI: **10.1016/j.seppur.2023.125117**.

6 Z. X. Zhong, G. W. Yu, W. T. Mo, C. J. Zhang, H. Huang, S. G. Li, M. Gao, X. J. Lu, B. P. Zhang and H. P. Zhu, Enhanced phosphate sequestration by Fe(iii) modified biochar derived from coconut shell, *RSC Adv.*, 2019, **9**, 10425–10436, DOI: **10.1039/c8ra10400j**.

7 D. Zhu, Y. Chen, H. Yang, S. Wang, X. Wang, S. Zhang and H. Chen, Synthesis and characterization of magnesium oxide nanoparticle-containing biochar composites for efficient phosphorus removal from aqueous solution, *Chemosphere*, 2020, **247**, 125847, DOI: **10.1016/j.chemosphere.2020.125847**.

8 X. X. Jia, T. Yin, Y. Wang, S. X. Zhou, X. Zhao, W. T. Chen and G. Z. Hu, Porous honeycomb cork biochar for efficient and highly selective removal of phosphorus from wastewater, *Biochar*, 2023, **5**, 14, DOI: **10.1007/s42773-023-00289-9**.

9 Y. K. Geng, Y. Wang, X. R. Pan and G. P. Sheng, Electricity generation and in situ phosphate recovery from enhanced biological phosphorus removal sludge by electrodialysis membrane bioreactor, *Bioresour. Technol.*, 2018, **247**, 471–476, DOI: **10.1016/j.biortech.2017.09.118**.

10 Y. Yang, J. Lohwacharin and S. Takizawa, Hybrid ferrihydrite-MF/UF membrane filtration for the simultaneous removal of dissolved organic matter and phosphate, *Water Res.*, 2014, **65**, 177–185, DOI: **10.1016/j.watres.2014.07.030**.

11 X. X. Jia, X. Zhao, Y. T. Zhou, F. Li, W. Liu, Y. M. Huang, H. C. Zhang, J. X. Ma and G. Z. Hu, Tri-functional lanthanum-based biochar for efficient phosphorus recovery, bacterial inhibition, and soil fertility enhancement, *Biochar*, 2023, **5**, 17, DOI: **10.1007/s42773-023-00216-y**.

12 M. L. Borno, D. S. Muller-Stover and F. Liu, Contrasting effects of biochar on phosphorus dynamics and bioavailability in different soil types, *Sci. Total Environ.*, 2018, **627**, 963–974, DOI: **10.1016/j.scitotenv.2018.01.283**.

13 M. Du, Y. Y. Zhang, Z. Y. Wang, M. R. Lv, Q. Xu, Z. Q. Chen, Q. X. Wen and A. Li, La-doped activated carbon as high-efficiency phosphorus adsorbent: DFT exploration of the adsorption mechanism, *Sep. Purif. Technol.*, 2022, **298**, 13, DOI: **10.1016/j.seppur.2022.121585**.

14 E. H. Sun, Y. Y. Zhang, Q. B. Xiao, H. Y. Li, P. Qu, C. Yong, B. Y. Wang, Y. F. Feng, H. Y. Huang, L. Z. Yang and C. Hunter, Formable porous biochar loaded with La-Fe(hydr)oxides/montmorillonite for efficient removal of phosphorus in wastewater: process and mechanisms, *Biochar*, 2022, **4**, 19, DOI: **10.1007/s42773-022-00177-8**.

15 H. Dong, J. Deng, Y. Xie, C. Zhang, Z. Jiang, Y. Cheng, K. Hou and G. Zeng, Stabilization of nanoscale zero-valent iron (nZVI) with modified biochar for Cr(VI) removal from aqueous solution, *J. Hazard. Mater.*, 2017, **332**, 79–86, DOI: **10.1016/j.jhazmat.2017.03.002**.

16 B. B. Qiu, Q. N. Shao, J. C. Shi, C. H. Yang and H. Q. Chu, Application of biochar for the adsorption of organic pollutants from wastewater: modification strategies, mechanisms and challenges, *Sep. Purif. Technol.*, 2022, **300**, 25, DOI: **10.1016/j.seppur.2022.121925**.

17 Y. Yin, Y. M. Xu, Z. Zhao, Y. N. Luan, Y. H. Xiao and C. Q. Liu, Nanoscale MgO confined in magnetic biochar via two-step

pyrolysis for enhanced phosphate adsorption, *Sep. Purif. Technol.*, 2024, **339**, 11, DOI: 10.1016/j.seppur.2024.126754.

18 W.-H. Chen, A. T. Hoang, S. Nižetić, A. Pandey, C. K. Cheng, R. Luque, H. C. Ong, S. Thomas and X. P. Nguyen, Biomass-derived biochar: from production to application in removing heavy metal-contaminated water, *Process Saf. Environ. Protect.*, 2022, **160**, 704–733, DOI: 10.1016/j.psep.2022.02.061.

19 K. Qian, A. Kumar, H. Zhang, D. Bellmer and R. Huhnke, Recent advances in utilization of biochar, *Renew. Sustain. Energy Rev.*, 2015, **42**, 1055–1064, DOI: 10.1016/j.rser.2014.10.074.

20 X. F. Tan, Y. G. Liu, Y. L. Gu, Y. Xu, G. M. Zeng, X. J. Hu, S. B. Liu, X. Wang, S. M. Liu and J. Li, Biochar-based nano-composites for the decontamination of wastewater: a review, *Bioresour. Technol.*, 2016, **212**, 318–333, DOI: 10.1016/j.biortech.2016.04.093.

21 A. Kumar, E. Singh, R. Mishra and S. Kumar, Biochar as environmental armour and its diverse role towards protecting soil, water and air, *Sci. Total Environ.*, 2022, **806**, 150444, DOI: 10.1016/j.scitotenv.2021.150444.

22 L. Zhang, L. B. Yang, M. C. Yang, X. G. You, Y. Y. Hong, Y. C. Yang, J. B. Chen, Y. Lin, Y. L. Zhang and X. F. Zhou, Phosphorus recovery from urine by CO_2-activated biochar for sustainable slow-release fertilizer applications: unveiling adsorption mechanisms by statistical physics modeling and predictive modeling with artificial neural networks, *Sep. Purif. Technol.*, 2024, **342**, 11, DOI: 10.1016/j.seppur.2024.126981.

23 M. K. Gratuito, T. Panyathanmaporn, R. A. Chumnanklang, N. Sirinuntawittaya and A. Dutta, Production of activated carbon from coconut shell: optimization using response surface methodology, *Bioresour. Technol.*, 2008, **99**, 4887–4895, DOI: 10.1016/j.biortech.2007.09.042.

24 B. Michalekova-Richveisova, V. Fristak, M. Pipiska, L. Duriska, E. Moreno-Jimenez and G. Soja, Iron-impregnated biochars as effective phosphate sorption materials, *Environ. Sci. Pollut. Res.*, 2017, **24**, 463–475, DOI: 10.1007/s11356-016-7820-9.

25 H. J. Xin, J. Yang, Y. Y. Lu, H. K. Xiao, H. T. Wang, K. M. Eltohamy, X. Q. Zhu, C. L. Liu, Y. Y. Fang, Y. Ye and X. Q. Liang, Potentials of emergent plant residue derived biochar to be alternative carbon-based phosphorus fertilizer by Fe(II)/Fe(III) magnetic modification, *Biochar*, 2024, **6**, 14, DOI: 10.1007/s42773-024-00300-x.

26 M. B. Ahmed, J. L. Zhou, H. H. Ngo, W. Guo and M. Chen, Progress in the preparation and application of modified biochar for improved contaminant removal from water and wastewater, *Bioresour. Technol.*, 2016, **214**, 836–851, DOI: 10.1016/j.biortech.2016.05.057.

27 J. S. Cha, S. H. Park, S.-C. Jung, C. Ryu, J.-K. Jeon, M.-C. Shin and Y.-K. Park, Production and utilization of biochar: a review, *J. Ind. Eng. Chem.*, 2016, **40**, 1–15, DOI: 10.1016/j.jiec.2016.06.002.

28 H. B. Liu, J. H. Shan, Z. B. Chen and E. Lichtfouse, Efficient recovery of phosphate from simulated urine by Mg/Fe bimetallic oxide modified biochar as a potential resource, *Sci. Total Environ.*, 2021, 784, DOI: 10.1016/j.scitotenv.2021.147546.

29 K. N. Palansooriya, S. Kim, A. D. Igalavithana, Y. Hashimoto, Y. E. Choi, R. Mukhopadhyay, B. Sarkar and Y. S. Ok, Fe(III) loaded chitosan-biochar composite fibers for the removal of phosphate from water, *J. Hazard. Mater.*, 2021, **415**, 125464, DOI: 10.1016/j.jhazmat.2021.125464.

30 Z. Wang, H. Guo, F. Shen, G. Yang, Y. Zhang, Y. Zeng, L. Wang, H. Xiao and S. Deng, Biochar produced from oak sawdust by lanthanum (La)-involved pyrolysis for adsorption of ammonium (NH_4^+), nitrate (NO_3^-), and phosphate (PO_4^{3-}), *Chemosphere*, 2015, **119**, 646–653, DOI: 10.1016/j.chemosphere.2014.07.084.

31 S. Wang, B. Gao, A. R. Zimmerman, Y. Li, L. Ma, W. G. Harris and K. W. Migliaccio, Removal of arsenic by magnetic biochar prepared from pinewood and natural hematite, *Bioresour. Technol.*, 2015, **175**, 391–395, DOI: 10.1016/j.biortech.2014.10.104.

32 B. Chen, Z. Chen and S. Lv, A novel magnetic biochar efficiently sorbs organic pollutants and phosphate, *Bioresour. Technol.*, 2011, **102**, 716–723, DOI: 10.1016/j.biortech.2010.08.067.

33 M. Lawrinenko, D. Jing, C. Banik and D. A. Laird, Aluminum and iron biomass pretreatment impacts on biochar anion exchange capacity, *Carbon*, 2017, **118**, 422–430, DOI: 10.1016/j.carbon.2017.03.056.

34 W. H. Wang, Y. Wang, P. L. Yang, M. Wang and K. Zhou, Physi-chemical mechanism and control effect of CaO_2 inhibiting phosphorus release from sediments under different dosing modes, *Chemosphere*, 2022, **303**, 135283, DOI: 10.1016/j.chemosphere.2022.135283.

35 Y. Qian, X. Zhou, Y. Zhang, W. Zhang and J. Chen, Performance and properties of nanoscale calcium peroxide for toluene removal, *Chemosphere*, 2013, **91**, 717–723, DOI: 10.1016/j.chemosphere.2013.01.049.

36 Y. Xu, F. E. Han, D. P. Li, J. Zhou and Y. Huang, Transformation of internal sedimentary phosphorus fractions by point injection of CaO_2, *Chem. Eng. J.*, 2018, **343**, 408–415, DOI: 10.1016/j.cej.2018.03.028.

37 J. Zhou, D. Li, Z. Zhao and Y. Huang, Phosphorus bioavailability and the diversity of microbial community in sediment in response to modified calcium peroxide ceramsite capping, *Environ. Res.*, 2021, **195**, 110682, DOI: 10.1016/j.envres.2020.110682.

38 H. Lu, S. Liu, A. Wang, H. Yang, X. Liang, X. Chen and Q. Li, Transmission and regulation insights into antibiotic resistance genes in straw-sludge composting system amended with calcium peroxide, *Bioresour. Technol.*, 2023, **386**, 129539, DOI: 10.1016/j.biortech.2023.129539.

39 M. V. Lopez-Ramon, F. Stoeckli, C. Moreno-Castilla and F. Carrasco-Marin, On the characterization of acidic and basic surface sites on carbons by various techniques, *Carbon*, 1999, **37**, 1215–1221, DOI: 10.1016/s0008-6223(98)00317-0.

40 T. Xiao, Y. Wang, J. N. Wan, Y. W. Ma, Z. C. Yan, S. H. Huang and C. Zeng, Fe-N-C catalyst with Fe-N_X sites anchored nano carboncubes derived from Fe-Zn-MOFs activate

peroxymonosulfate for high-effective degradation of ciprofloxacin: thermal activation and catalytic mechanism, *J. Hazard. Mater.*, 2022, **424**, 14, DOI: 10.1016/j.jhazmat.2021.127380.

41 C. Affolter-Zbaraszczuk, H. Ozcelik, F. Meyer, O. Gallet, P. Lavalle, V. Ball, C. M. Ghimbeu, P. Schaaf and H. Knopf-Marques, Hybrid extracellular matrix microspheres for development of complex multicellular architectures, *RSC Adv.*, 2017, **7**, 5528–5532, DOI: 10.1039/c6ra27680f.

42 D. Mohan, K. Abhishek, A. Sarswat, M. Patel, P. Singh and C. U. Pittman, Biochar production and applications in soil fertility and carbon sequestration – a sustainable solution to crop-residue burning in India, *RSC Adv.*, 2018, **8**, 508–520, DOI: 10.1039/c7ra10353k.

43 Z. Sun, X. D. Wu, C. K. Russell, M. D. Dyar, E. C. Sklute, S. Toan, M. H. Fan, L. B. Duan and W. G. Xiang, Synergistic enhancement of chemical looping-based CO_2 splitting with biomass cascade utilization using cyclic stabilized $Ca_2Fe_2O_5$ aerogel, *J. Mater. Chem. A*, 2019, **7**, 1216–1226, DOI: 10.1039/c8ta10277e.

44 D. Jiang, B. Chu, Y. Amano and M. Machida, Removal and recovery of phosphate from water by Mg-laden biochar: batch and column studies, *Colloid. Surface.*, 2018, **558**, 429–437, DOI: 10.1016/j.colsurfa.2018.09.016.

45 S. Y. Lee, J.-W. Choi, K. G. Song, K. Choi, Y. J. Lee and K.-W. Jung, Adsorption and mechanistic study for phosphate removal by rice husk-derived biochar functionalized with Mg/Al-calcined layered double hydroxides via co-pyrolysis, *Compos. B Eng.*, 2019, **176**, 107209, DOI: 10.1016/j.compositesb.2019.107209.

46 M. Mallet, K. Barthelemy, C. Ruby, A. Renard and S. Naille, Investigation of phosphate adsorption onto ferrihydrite by X-ray photoelectron spectroscopy, *J. Colloid Interface Sci.*, 2013, **407**, 95–101, DOI: 10.1016/j.jcis.2013.06.049.

47 X. Cui, H. Hao, Z. He, P. J. Stoffella and X. Yang, Pyrolysis of wetland biomass waste: potential for carbon sequestration and water remediation, *J. Environ. Manage.*, 2016, **173**, 95–104, DOI: 10.1016/j.jenvman.2016.02.049.

48 P. Singh, S. Rawat, N. Jain, A. Bhatnagar, P. Bhattacharya and A. Maiti, A review on biochar composites for soil remediation applications: comprehensive solution to contemporary challenges, *J. Environ. Chem. Eng.*, 2023, **11**, 110635, DOI: 10.1016/j.jece.2023.110635.

49 Y. H. Zou, R. Y. Zhang, L. Y. Wang, K. Xue and J. G. Chen, Strong adsorption of phosphate from aqueous solution by zirconium-loaded Ca-montmorillonite, *Appl. Clay Sci.*, 2020, **192**, 105638, DOI: 10.1016/j.clay.2020.105638.

50 F. Hu, M. Wang, X. Peng, F. Qiu, T. Zhang, H. Dai, Z. Liu and Z. Cao, High-efficient adsorption of phosphates from water by hierarchical CuAl/biomass carbon fiber layered double hydroxide, *Colloid. Surface.*, 2018, **555**, 314–323, DOI: 10.1016/j.colsurfa.2018.07.010.

51 M. D. Khan, T. Chottitisupawong, H. H. T. Vu, J. W. Ahn and G. M. Kim, Removal of Phosphorus from an Aqueous Solution by Nanocalcium Hydroxide Derived from Waste Bivalve Seashells: Mechanism and Kinetics, *ACS Omega*, 2020, **5**, 12290–12301, DOI: 10.1021/acsomega.0c00993.

52 Y. Feng, Y. Luo, Q. He, D. Zhao, K. Zhang, S. Shen and F. Wang, Performance and mechanism of a biochar-based Ca-La composite for the adsorption of phosphate from water, *J. Environ. Chem. Eng.*, 2021, **9**, 105267, DOI: 10.1016/j.jece.2021.105267.

53 T. Liao, T. Li, X. Su, X. Yu, H. Song, Y. Zhu and Y. Zhang, $La(OH)_3$-modified magnetic pineapple biochar as novel adsorbents for efficient phosphate removal, *Bioresour. Technol.*, 2018, **263**, 207–213, DOI: 10.1016/j.biortech.2018.04.108.

54 N. Zhu, T. Yan, J. Qiao and H. Cao, Adsorption of arsenic, phosphorus and chromium by bismuth impregnated biochar: adsorption mechanism and depleted adsorbent utilization, *Chemosphere*, 2016, **164**, 32–40, DOI: 10.1016/j.chemosphere.2016.08.036.

55 J. Li, B. Li, H. Huang, X. Lv, N. Zhao, G. Guo and D. Zhang, Removal of phosphate from aqueous solution by dolomite-modified biochar derived from urban dewatered sewage sludge, *Sci. Total Environ.*, 2019, **687**, 460–469, DOI: 10.1016/j.scitotenv.2019.05.400.

56 Z. Ajmal, A. Muhmood, R. J. Dong and S. B. Wu, Probing the efficiency of magnetically modified biomass-derived biochar for effective phosphate removal, *J. Environ. Manage.*, 2020, **253**, 10, DOI: 10.1016/j.jenvman.2019.109730.

57 S. N. Zhuo, T. C. Dai, H. Y. Ren and B. F. Liu, Simultaneous adsorption of phosphate and tetracycline by calcium modified corn stover biochar: performance and mechanism, *Bioresour. Technol.*, 2022, **359**, 127477, DOI: 10.1016/j.biortech.2022.127477.

58 Q. Cui, J. Xu, W. Wang, L. Tan, Y. Cui, T. Wang, G. Li, D. She and J. Zheng, Phosphorus recovery by core-shell γ-Al_2O_3/Fe_3O_4 biochar composite from aqueous phosphate solutions, *Sci. Total Environ.*, 2020, **729**, 138892, DOI: 10.1016/j.scitotenv.2020.138892.

59 W. P. Zhang, M. Y. Sun and R. Prins, Multinuclear MAS NMR identification of fluorine species on the surface of fluorinated γ-alumina, *J. Phys. Chem. B*, 2002, **106**, 11805–11809, DOI: 10.1021/jp0212489.

60 B. L. Wu, J. Wan, Y. Y. Zhang, B. C. Pan and I. M. C. Lo, Selective Phosphate Removal from Water and Wastewater using Sorption: Process Fundamentals and Removal Mechanisms, *Environ. Sci. Technol.*, 2020, **54**, 50–66, DOI: 10.1021/acs.est.9b05569.

61 Y. Fang, A. Ali, Y. Gao, P. Zhao, R. Li, X. Li, J. Liu, Y. Luo, Y. Peng, H. Wang, H. Liu, Z. Zhang and J. Pan, Preparation and characterization of MgO hybrid biochar and its mechanism for high efficient recovery of phosphorus from aqueous media, *Biochar*, 2022, **4**, 40, DOI: 10.1007/s42773-022-00171-0.

62 X. Y. Li, Y. H. Xie, F. Jiang, B. Wang, Q. L. Hu, Y. Tang, T. Luo and T. Wu, Enhanced phosphate removal from aqueous solution using resourceable nano-CaO_2/BC composite: behaviors and mechanisms, *Sci. Total Environ.*, 2020, **709**, 12, DOI: 10.1016/j.scitotenv.2019.136123.